

# 1 Balloon drift estimation and improved position estimates for 2 radiosondes

3 Ulrich Voggenberger<sup>1</sup>, Leopold Haimberger<sup>1</sup>, Federico Ambrogi<sup>1</sup>, Paul Poli<sup>2</sup>

4 <sup>1</sup>Department of Meteorology and Geophysics, University of Vienna, Vienna, 1090, Austria

5 <sup>2</sup>European Centre for Medium-Range Weather Forecasts, Bonn, Germany

6 *Correspondence to:* Ulrich Voggenberger (ulrich.voggenberger@univie.ac.at)

## 7 **Abstract.**

8 When comparing model output with historical radiosonde observations, it is usually assumed that the radiosonde has risen  
9 exactly above its starting point and has not been displaced by the wind. This has changed only relatively recently with the  
10 availability of Global Navigation Satellite System (GNSS) receivers aboard the radiosondes in the late-1990s, but even then  
11 the balloon trajectory data were often not transmitted, although this information was the basis for estimating the wind in the  
12 first place. Depending on the conditions and time of year, radiosondes can sometimes drift a few hundred kilometres,  
13 particularly in the mid-latitudes during the winter months. The position errors can lead to non-negligible representation  
14 errors when the corresponding observations are assimilated.

15 This paper presents a methodology to compute changes in the balloon position during its vertical ascent, using only limited  
16 information, such as the vertical profile of wind contained in the historical observation reports. The sensitivity of the method  
17 to various parameters is investigated, such as the vertical resolution of the input data, the assumption about vertical ascent  
18 speed of the balloon, and the departure of the surface of the Earth from a sphere. The paper considers modern GNSS sonde  
19 data reports for validation, for which the full trajectory of the balloon is available, alongside the reported wind. Evaluation is  
20 also conducted by comparison with ERA5 and by conducting low-resolution data assimilation experiments. Overall, the  
21 results indicate that the trajectory of the radiosonde can be accurately reconstructed from original data of varying vertical  
22 resolution and that the more accurate balloon position reduces representation errors, and, in some cases, also systematic  
23 errors.

24 **1 Introduction**

25

26 Prior to the availability of remote sensing techniques, upper-air measurements of air motions were widely collected using  
 27 Lagrangian perspectives, with weather balloons (e.g., Dutton, 1986). The uncertainty of such upper -air observations  
 28 depends not only on the measurements themselves but also on the availability and quality of associated metadata and  
 29 measurement position: this is generally associated with so-called representation errors (e.g., Kitchen, 1989). As weather  
 30 balloons drift with the wind during their travel, including ascent, they can thus be displaced over large distances (**Figure 1**),  
 31 in some cases more than 400 km from their launch base (e.g., Seidel et al., 2011). Precise knowledge of the balloon position  
 32 is particularly important in regions of [sharpsteep](#) horizontal gradients, e.g. near mountain ranges or near jet streams.  
 33 Tschannett (2003) and Steinacker et al. (2005) noted that apparent superadiabatic vertical lapse rates in Foehn events  
 34 disappeared after the balloon displacement had been taken into account. For operational monitoring, detailed information  
 35 regarding the balloon trajectory was generally not recorded or not transferred via the data distribution networks until the  
 36 advent of Global Navigation Satellite Systems (GNSS). Even later, when GNSS sensors became available, the information  
 37 collected was often not transmitted, although the wind data was calculated directly from it (WMO, 2021), as there was no  
 38 available space in the alphanumeric codes. This became possible with the (ongoing) migration from alphanumeric codes to  
 39 Binary Universal Form for the Representation of meteorological data (BUFR), allowing also the reporting of many more  
 40 levels in the vertical (Ingleby et al., 2016). Only since the mid-2000s efforts have been made to take into account is the  
 41 balloon drift taken into account in modern observation processing of GNSS sondes, with beneficial results (e.g., Keyser,  
 42 2000; Laroche and Sarrazin, 2013; Ingleby [et al.](#), 2018).

43

44 Radiosonde measurements are used in a variety of applications, including near-real-time by forecasters and Numerical  
 45 Weather Prediction (NWP), but also for air pollution or other scientific investigations, including climate monitoring (e.g.,  
 46 Dabberdt and Turtiainen, 2015). The production of climate reanalyses that directly assimilate radiosonde observations, such  
 47 as ERA5 (Hersbach et al. 2020), is expected to benefit from more accurate historical balloon position data, similarly to  
 48 NWP. In this regard, the location precision of the assimilated measurements should be commensurate with the horizontal  
 49 resolution (~10 to 20 km globally) of future next-generation reanalyses (~10 to 20 km globally, e.g., Hersbach et al., 2022).  
 50 At such resolutions, assuming vertical ascents for a balloon that is displaced by a couple of hundred kms would amount to  
 51 comparing the balloon measurements with model values that are 10 or more grid boxes away, which is clearly suboptimal.  
 52 Resolving this situation requires, for historical soundings, to reconstruct the balloon trajectories from the little information  
 53 that is available (Stohl, 1998). In many cases, this information only consists in the vertical profile of wind, as discussed later  
 54 in the paper.

56 Section 2 describes the data and a method to calculate the balloon drift from historical radiosonde ascent data. Details of the  
 57 technical implementation, with python code and test data, are provided in section 3. Section 4 presents validation results,

58 including several sensitivity analyses to explore the robustness and accuracy of the approach. Sections 5 and 6 show  
 59 evaluation results, using two different approaches, whereby the beneficial impact of the more accurate balloon position is  
 60 demonstrated. Section 7 includes a discussion and conclusions.

61 **2 Data and methodology**

62

63 **2.1 Radiosonde data**

64 Radiosonde data used in this work are obtained from the Integrated Global Radiosonde Archive (IGRA), Version 2 (Durre et  
 65 al., 2016) and via the Copernicus Climate Change Service (C3S) Climate Data Store (CDS). High-resolution radiosonde data  
 66 used for validation are obtained in BUFR format from the National Centers for Environmental Information Radiosonde  
 67 Archive (NOAA NCEI).

68

69 The quality of the available wind data depends on their encoding and the method used to track the balloons. Measuring  
 70 techniques for upper- air winds have changed significantly over time, with a clear general trend towards improvements in  
 71 quality, thanks to removal of procedural errors, in particular (e.g., Crutcher, 1979), noting also improvements in the accuracy  
 72 of encoding, with evolution of the data formats. All these changes are described in the WMO Publication Nr. 8, Guide to  
 73 Meteorological Instruments and Methods of Observation, published since 1954 by the WMO Commission for Instruments  
 74 and Methods of Observation (CIMO; WMO, 2021). Regarding changes in the measurements of wind and balloon positions,  
 75 there are three important distinctions to be made.

76

77 The first distinction concerns the sensing apparatus: non-GNSS versus GNSS sondes. Early observations used only ground-  
 78 based tracking, e.g., by theodolite, which was fairly accurate but could lose the balloon early during cloudy or highstrong  
 79 wind speed conditions, and relied on an assumed ascent rate if, like in most cases, a single theodolite was used (e.g., Favà et  
 80 al., 2021). From the mid-1950s onward, radar tracking or radio-positioning of the radiosonde became standard. Wind  
 81 components were then calculated from the measured position and time differences.

82 In the 1990s, GNSS modules were introduced, which can track the horizontal and vertical position of the sensor at high  
 83 frequency, thanks to improvements and miniaturisation of the electronics. The resulting data were then used to calculate the  
 84 wind variables in the data set, but the position data were not transmitted to the global network and are therefore not available  
 85 in the used inputglobal databases in most cases until 2014.

86 The higher frequency of observations exchanged in recent years can expose the pendulum motion of the sonde beneath the  
 87 balloon in its observed position (Ingleby et al, 2022). In our experimental cases, we did not observe any significant effect of

88 the pendulum motion, its magnitude is muchbeing generally much smaller than the wind advection displacements,  
 89 suggesting it does not appear to need to be taken into account to first order.

90

91 The second aspect is the determination of altitude. Prior to GNSS observations, altitude was determined by three different  
 92 methods: ascent speed estimation, pressure sensors, and vertical radar or radio-positioning, with continued efforts to increase  
 93 the quality of observations over time. Ascent speed can be affected by many factors, and Murillo et al. (2005) estimated a  
 94 scatter in linear ascent rates of about 5% about the mean value for pilot balloons, after using double theodolites to conduct  
 95 measurements to measure the balloon height during ascent.

96

97 The third aspect is the data format used for transmission. Essentially two main message systems have been used to transmit  
 98 the observed radiosonde data: Traditional Alphanumeric Code (TAC) and BUFR. The main difference is that BUFR allows  
 99 not only for a much higher vertical resolution (up to 1 second frequency, corresponding to approximately 5 m altitude  
 100 difference), but also for a higher coding precision. The BUFR messages report wind direction with a resolution of 1- degree,  
 101 whereas TAC messages report wind direction to the nearest 5-degrees. Also In addition, time and three-dimensional position  
 102 information is only transmitted via BUFR but not with via TAC. TAC messages typically also include data only on  
 103 mandatory and significant levels. Mandatory levels are a set of predefined pressure levels. Significant levels for wind are  
 104 added as needed before transmission so that the wind speed does not deviate by more than 5 m/s from linearly-interpolated  
 105 values, according to the above-cited WMO CIMO guide.

106 There are also thermodynamically significant levels, which refer to specific levels of atmospheric pressure at which  
 107 significant changes in temperature, humidity or other thermodynamic properties occur. Most transmitted radiosonde profiles  
 108 include some of these.

## 109 **2.2 Quality control**

110 The following steps are taken to exclude outliers:

- 111 • For wind speed, we applied a range check, with The wind speed is limited to 150 m/s, a value that is rarely reached,  
 112 even in strong upper-level jets.
- 113 • For temperature, needed for geopotential calculations, we relied on the IGRA2 quality control (Durre et al. 2018)  
 114 that already removes gross errors. AAn\_additional very cruderange check was also applied, with (temperature  
 115 limited to between 173 and 373 K) was applied, just to verify that the data were read correctly and avoid possible  
 116 encoding errors in the messages. The temperature is limited to values between 173 K and 373 K.

117 Observations that fall outside these limits are not processed further, to avoid degrading the quality of the output (balloon  
 118 trajectory).

119 It was investigated whether additional quality control measures would improve performance and the validation of the RMSE  
 120 differences discussed in section 5. To improve outlier removal, we filtered the observations based on the 1st and 99th

11

12

121 percentiles of the differences observations minus the [ERA5](#) forecast (these differences are called background [departures afterwards](#)) forecast differences background from the ERA5 feedback. This was completed in two stages: once for each level,  
 122 and then again for the entire set of available wind speed and temperature data. However, neither of the two versions  
 123 improved the RMSE differences. Rather, we found that the background departures were often large enough to be discarded  
 124 just in the interesting cases of strong but plausible displacements. The reason was not always the displacements themselves  
 125 but also the fact that large lateral displacements can lead to large height errors in profiles from non-GNSS Russian  
 126 radiosondes, since those have no pressure sensor but rely on radar heights (Kats et al. , 2005). However even for these  
 127 sondes, we found that taking into account the balloon drift reduces the differences to the ERA5 background forecasts.  
 128  
 129 The results presented in section 6 include the standard quality controls applied during data assimilation experiments, as  
 130 detailed in the technical documentation published by ECMWF (2023).

131

132

133

134 Filtering radiosonde input data before the displacement calculation based on the number of available observations per profile  
 135 is recommended. A profile should not be too coarse and should not start too high above the ground. For the experiments  
 136 conducted in this study, the limit for the initial observation was set at 1500 m above the release station height.

### 137 2.3 Estimation of the balloon trajectory

138 The balloon position is calculated relative to the launch position (so-called base coordinates), as latitude displacement and  
 139 longitude displacement (decimal degrees). For each vertical level, these two values can be added to the base coordinates to  
 140 obtain the new (latitude, longitude) position at the given level. The same approach applies to the reconstruction of the  
 141 measurement times at all levels. This practice conforms to the BUFR encoding standard.

142

143 For the position calculation, the same simple physical laws that have been used to derive the reported wind components are  
 144 applied. Only a few initial parameters are necessary for this:

145

146
 

- 147 station coordinates or starting point of the sonde, (latitude and longitude) here called base coordinates [latitude and longitude](#);
- 148 wind vector (zonal and meridional components, noted respectively u and v), measured by the sonde at different  
 149 pressure levels;
- 150 measurement time (t) at different pressure levels.

151

152 These variables enable calculation of how long the sonde was exposed to horizontal wind, and therefore can be used to  
 153 estimate the displacement of the sonde.

14

15

154 Especially older datasets often only contain the starting time of the ascent, time information is not available for any of the  
 155 reported pressure levels.

156 To estimate the time elapsed since the release of the balloon, three variables are needed:

157

158 • the reported pressure levels (generally available from radiosondes) or heights (generally available from so-called  
 159 PILOT balloons, also called PIBAL),  
 160 • the sonde ascent speed.  
 161 • the surface pressure or station height (not strictly needed for displacement calculation since first level is typically  
 162 reported quite close to the surface)

163

164 PILOT or PIBAL profiles provide an estimate of height at each level, from which the time at each level can be reconstructed,  
 165 assuming a given ascent speed. However, for multivariate soundings (radiosondes reporting temperature and wind), observed  
 166 pressure is often the only information available regarding the radiosonde vertical position. In such a case, the pressure profile  
 167 needs to be transformed to a height profile. This can be done assuming a piecewise constant temperature gradient between  
 168 the levels in layers of the profile. The calculation of the vertical gradient of temperature with respect to altitude from the  
 169 vertical gradient of temperature with respect to pressure is shown below in **Formulae 1** and **2**. Subsequently, **Formula 3**  
 170 indicates how this information is used to determine the heights of all pressure levels. If the height information is already  
 171 available (e.g. PILOT data), those steps can be skipped.

172

173 The vertical resolution of the available data varies. While early ascents often contain even less than the mandatory levels (16  
 174 levels), recent data in high resolution BUFR are available on 3000 levels or more. The sensitivity of displacement  
 175 calculations to vertical resolution is investigated later in this paper.  
 176 If a single mandatory level is missing within the ascent range, then the displacements are not calculated; we consider that too  
 177 much information is missing in such a case. If a level was not mandatory in historical data (e.g. 70 hPa, 250 hPa, 925 hPa),  
 178 this rule does not apply to the data. However, an early termination of the vertical ascent is not an issue, then the  
 179 displacements are only calculated up to the highest available level.

180

181 The determination of the sonde's ascent speed is more uncertain. It depends on some variables that are poorly determined or  
 182 unknown, such as the air vertical wind speed and the weight to buoyancy ratio of the probe and the balloon. Deviations in the  
 183 filling level of the balloon, the air resistance of the balloon skin, as well as the ambient temperature and the balloon gas  
 184 temperature further influence the ascent speed. A review of some of these factors was made by Favà et al. (2021).

185

186 Using data from recent sondes, our study of the data with known altitude time series indicates that the rate of ascent varies  
 187 mostly between 2 and 10 m/s. Within this large range, **Figure 2** shows that the mode of the distribution of ascent speeds is

17

18

188 | around 5 m/s. **Table 13** further indicates that the interquartile range is 2 m/s (i.e., from 4 m/s to 6 m/s). These findings are  
 189 consistent with other sources (e.g., Seidel et al., 2011). These statistics represent global fluctuations in the ascent speed of  
 190 weather balloons.

191

192 Over short time scales, **Figure 3** indicates the vertical velocity of the probe fluctuates substantially. This is true both within a  
 193 single ascent and also between different ascents. Near the ground and above the tropopause the fluctuations are largest.

194

195 Given the considerations above for historical balloons, one must recognize that the vertical speed can only be estimated in  
 196 most cases, and will always lead to significant deviations as compared to measurements obtained from high- resolution  
 197 dataascents. Note the high vertical resolution shown in **Figure 3** is hardly reached in ascents before the year 2000. This also  
 198 means that if only mandatory levels are available, the fluctuations in average ascent speed at each available level are  
 199 smaller, due to the longer averaging intervals.

200

201 **Figure 2** and **Figure 3** show that an assumed ascent rate of 5 m/s agrees well with the observed mean value. To counteract  
 202 the effects of this fluctuating parameter, an attempt was made to use a height-dependent function instead of a constant speed,  
 203 which represents the annual average over more than 100 stations.

204

205 As part of this experiment, a polynomial model was also tried, used in an attempt to improve the accuracy of the average  
 206 ascent speed. Improved accuracy is measured by a better fit with observed ascent speeds of BUFR data. The resulting  
 207 displacements showed, however, very little improvement (i.e. smaller differences to GNSS measured displacements),  
 208 indicating that the assumed vertically constant ascent rate of 5 m/s is a sufficient approximation.

209

210 As a next step, it is necessary to calculate the height profile from temperature and pressure information. For this step, we  
 211 using use the formula for a dry atmosphere with piecewise constant lapse rate (Alexander and de la Torre, P., 2011). Relative  
 212 humidity could also be considered by using the virtual temperature, but, since it is often not available for early ascents and  
 213 we also found that the differences in resulting displacements were small, the air temperature is used in the equation of state.  
 214 For the first level, the International Civil Aviation Organization (ICAO) standard atmosphere lapse rate of -0.0065 K/m is  
 215 used. For all subsequent steps, the temperature gradient is calculated directly from the temperature and pressure profile  
 216 (mean values for each layer “i”).

217

218 The height profile is then used to calculate the time interval spent by the sonde between the noted levels. It can be estimated  
 219 using the estimated vertical velocity mentioned earlier.

220 These time intervals are then used to determine the transport of the balloon according to the mean wind inside the layer  
 221 between the levels  $i$  to  $i + 1$ , see **Formula 4**.

20

21

22

222

223 Afterwards, this distance is converted into latitude and longitude using either the inverse Haversine method on an assumed  
 224 sphere, or the forward transport function on the "WGS84" ellipsoid. The difference between the two transport functions is  
 225 found to be practically invisible for smaller observed displacements (see **Figure 4**). Nevertheless, the ellipsoid option is used  
 226 as it should deliver higher accuracy results. Finally, the resulting latitudes and longitudes are subtracted from the base  
 227 coordinates to obtain the displacements.

228

229 Particular care is required when using reported wind direction near the North or South Pole. For example, when crossing the  
 230 North Pole, a radiosonde in a southerly airflow (prior to the crossing) finds itself in a northerly airflow (afterwards). So far,  
 231 only TAC has been used at the South Pole station, which means that the wind components are reported according to the  
 232 launch position, not to the actual position, and is thus constant during the ascent. We calculate the displacements in x and y  
 233 direction valid at this position and then convert that back to lat/lon positions and displacements.

234 The WMO Manual on Codes states that for stations within 1° of either pole wind direction shall be reported in such a way  
 235 that the azimuth ring shall be aligned with its zero coinciding with the Greenwich 0° meridian. There is currently an attempt  
 236 to update this advice for BUFR reports, such that wind direction should be reported relative to the current reported longitude  
 237 - to help in NWP use of such winds. Before comparing winds from the South Pole station with NWP fields they should have  
 238 their direction adjusted when the drift positions are calculated, but note (this was not currently done in the present work).  
 239 The displacement calculations data have been checked specifically for this issue and no problems were found.

240 Although the principle of displacement calculation is similar to the method presented in earlier work on this topic (Laroche  
 241 and Sarrazin, 2013), we use different input data for height information. Instead of using the average ascent time for each  
 242 standard level, we calculate the times for each available level using the mean lapse rate for the representative layer.  
 243 Aberson (2017) applied a similar approach for dropsondes, albeit with a different way of calculating the vertical velocity.  
 244 Both of these methods are successful and promising, and for the purpose of this method they have been used as the basis for  
 245 reconstructing the trajectories as best as possible.

### 247 3 Implementation and availability

248 The software necessary for the creation of calculated balloon trajectories can be found in the Python package rs-drift:

249 • <https://zenodo.org/records/10663306>  
 250 • <https://pypi.org/project/rs-drift/>

251 Examples on how to use it are available in all repositories as an IPython notebook "rs\_drift\_example.ipynb".

252

23

24

253 In addition to the coordinates of the launch site or station in degrees latitude and longitude, the trajectory function requires  
254 profiles of four input variables in the right units: temperature [K], pressure [Pa], zonal wind (u) [m/s], meridional wind (v)  
255 [m/s]. It accepts only input which is sorted in ascending order.

```
256 trajectory = rs_drift.drift.trajectory(lat,lon,temperature,u,v,pressure)
```

257 The function returns the following output:

```
258 trajectory == [latitude_displacement, longitude_displacement, seconds_since_start]
```

259 All those output variables are numpy arrays, with one element for each pressure level - with the same length as the input  
260 data. For PIBAL ascents, the geopotential height must be provided as an additional keyword parameter.

261

262 It is possible to experiment with input data. If humidity information is available, the virtual temperature can be used instead  
263 of the observed air temperature. Also if more information of the balloon's mean ascent rate is present, this should be used as  
264 input in the additional arguments. Any approach including proper quality control of input data that is available should be  
265 used to create the best possible estimation of the balloon drift.

266

267 The drift of the balloon and sonde compounds is introduced as "displacement" from the starting point (launch site). For  
268 simplicity, the displacements can be added to the base coordinates to obtain the vertical profile of positions of the balloon.

269

## 270 **4. Validation with GNSS radiosondes**

271 Validation per se is only possible when a trusted source can provide a good reference. Such is the case for modern sondes  
272 equipped with GNSS receivers, when it comes to the recovery of the balloon trajectories. For pre-GNSS radiosondes, a  
273 similar validation would be possible, if only one had available the information about the balloon trajectory. Unfortunately,  
274 this information is available only in rare cases.

275

276 The data from the modern GNSS radiosonde data encoded in the recent high-resolution BUFR files are used to verify the  
277 systematic and random errors of the calculated displacements at different pressure levels. This data set contains second-by-  
278 second records of actual positions of the sonde measured by GNSS in the form of displacements, thus enabling the direct  
279 comparison with the calculated displacements.

280

281 **Figure 4** also shows that the displacements obtained from GNSS and the displacements calculated from the wind data agree  
282 quite well. The small deviations likely come from differences between the actual (unknown) and assumed (5 m/s) ascent  
283 rate.

284

285 **Figure 5** provides an overview how large the displacements typically are and gives profiles of uncertainty estimates for the  
 286 calculated displacements. In the troposphere the RMSE is mostly below 0.02 degrees (2.5 km), in the stratosphere it can be  
 287 up to 0.1 degrees (12 km). These numbers amount to uncertainties of about one part in five to ten, of the observed variations  
 288 (RMS), in the example shown. Still, this is much better than just ignoring the displacement.

289

290 These results were obtained by using as input the high-resolution data. For historical radiosondes, only comparatively low-  
 291 resolution information is available (in the form of mandatory plus significant levels).

292 In **Figure 6** and **Figure 7**, the impact of using only mandatory and significant level information is shown. The difference of  
 293 displacements in **Figure 6** is minimal, although the displacement is relatively large.

294 **Figure 7** shows a case of larger differences in relative terms. The overall zonal displacements are large and the winds vary  
 295 strongly with altitude. An issue arises when selecting data points with low representativeness from the ascent, particularly  
 296 those that are far from the layer average. This can result in less accurate outcomes compared to using averages from less  
 297 detailed data. Figure 7 provides a good example of this issue with the v component of wind at original resolution and  
 298 mandatory pressure levels only. The method of calculating the displacements itself uses mean wind speeds within the  
 299 considered levels. Thus, if the observations are also means of larger vertical height differences, more or less randomly  
 300 observed peaks become a smaller source of error.

301 Figures 6 and 7 respectively show the range of accuracy of the calculated trajectories quite well. The final displacements  
 302 may differ in quality depending on the quality of the observations, the representativeness of the available levels, and the  
 303 vertical resolution. All ascents in the validation examples had displacements, which added value in bringing the observation  
 304 closer to the true position. The accuracy may vary based on the aforementioned input variables. However, we did not find  
 305 any case where using the displacements would lead to a worse position estimate.

306

307 **Figure 8** shows the comparison between the displacements of two different data sets - on high resolution BUFR levels and  
 308 on the other hand on mandatory levels only. It can be seen that for this subset of ascents there is still much value in the  
 309 displacements for the mandatory levels only version. However, it should be noted that more available levels always lead to  
 310 better results and the highest possible number should be used in any case.

311

312 Many of the older observational reports contain temperature and wind data on different levels. Only at mandatory levels both  
 313 variables are available. In this case, interpolation can be performed for the points in between. When applied to IGRA data,  
 314 wind data are interpolated to levels of the temperature observations. This allows the input to be maximised to calculate the  
 315 best possible displacements.

316

317 **5. Evaluation with ERA5**

318 To evaluate the impact of taking the displacements into account, we compared the observed values from the radiosondes  
 319 with the gridded ERA5 data, in one case assuming a strictly vertical ascent, and in the other case assuming an ascent along  
 320 the calculated (slanted) trajectory defined by the displacements. The ERA5 fields at hourly resolution and  $1^\circ \times 1^\circ$  horizontal  
 321 resolution were interpolated linearly horizontally to the observations locations defined in either of the two cases mentioned  
 322 earlier (vertical or slanted).

323 These tests and comparisons used the short term forecast of the ERA5 assimilating model, also referred to as "background".  
 324 This choice, instead of using ERA5 analyses, was made to try to maintain as much independence as possible with respect to  
 325 the observations. This choice should largely avoid possible problems resulting from the fact that the observations are also  
 326 assimilated into the ERA5 data, given that many other observations were assimilated alongside radiosondes and also  
 327 influenced the analysis state. Experimental comparisons to the ERA5 analyses (in contrast to background forecasts) showed  
 328 that the analysis data fits significantly better with the vertical trajectory of observation than with the slanted version. This is  
 329 to be expected, since radiosondes were assimilated as vertical profiles in ERA5.

330

331 **Figure 9** shows the benefit of comparing the radiosonde observations with the *background forecasts* as slanted profiles  
 332 instead of vertical profiles. In low layers (below 700 hPa), the displacements are relatively smaller than at higher levels, and  
 333 therefore hardly lead to deviations for temperature. In most cases, there is an improvement at levels located above 750 hPa,  
 334 though at some stations the improvement is visible already as soon as the sonde reaches 850 hPa, depending on the wind  
 335 speed and topography around the station. Typically, the effect is largest in regions with high upper-level wind speeds.  
 336 Taking the displacements into account improves the background departure statistics between measurements and ERA5 not  
 337 only for temperature but also wind and relative humidity.

338

339 For relative humidity, the improvement is confined to levels located below 250 hPa. Above this level, the relative humidity  
 340 is generally very low, making it difficult to detect any meaningful difference with respect to the ERA5 background.

341 It is also important to note that some stations, where the RMSE of the ascents do not show signals of improvement in  
 342 temperature, often still show improvement in humidity or wind (or vice versa).

343

344 Considering that radiosonde observations make up a larger part of the total observations for the reanalysis in earlier years,  
 345 one might think that especially for these years the displacements are more relevant. The data investigation reveals that  
 346 improvements of the departure statistics are not greater for earlier ascents than for more recent ascents. The reason might be  
 347 that reanalysis fields before the satellite era are more strongly dependent on radiosondes. At these times few other upper-air  
 348 observations were available, and radiosonde data were assimilated assuming vertically straight ascents. However, the density  
 349 of the input data and the general quality of the reanalysis increased over the time, while the bias in measurements of the

350 uppermost levels decreased over time. Therefore, the relative importance of representation uncertainties, with respect to the  
 351 two other sources of uncertainties in the comparison (radiosonde instrumental uncertainties and ERA5 background  
 352 uncertainties), is larger for more recent ascents. **Figure 10** shows that considering the displacements is beneficial, although  
 353 to a lesser extent, also in the early days, when little upper- air information other than radiosondes was available.

354

355 Finally, in **Figure 11** there are the results of a global comparison for the year 2000 - like the previous ones, but calculated for  
 356 all the available stations. A positive difference again indicates improvement due to taking the displacements into account.

357

358 To give a better insight, the differences of the RMSE are also plotted on a map for the 150 hPa level in **Figure 12**. Warm  
 359 colours show improvement for the respective station by applying the displacements, cold colours show a deterioration.  
 360 Improvement clearly predominates for the majority of stations. Deteriorations in quality appear less frequent and of smaller  
 361 magnitudes than improvements.

362

363 **Figure 13** shows the difference of the ERA5 background eastward wind speed in the 1990s at the station location minus the  
 364 same wind speed at the displaced location. The differences are sizable in some regions. For example, the weaker wind speeds  
 365 above station locations in China would indicate systematically too high observed wind speeds. This effect is large enough to  
 366 explain some of the radiosonde wind minus background wind differences, as pointed out by Tenenbaum et al. (2022). This  
 367 stresses again the importance of avoiding position errors in historical radiosonde ascents. Without the adjustments, artificial  
 368 trends in wind speed from radiosondes would be introduced in some regions when switching from traditional to GNSS  
 369 radiosondes.

370

## 371 **6. Evaluation with data assimilation experiments**

372 Desroziers et al. (2005) proposed a method to diagnose uncertainty statistics of observations in a data assimilation  
 373 framework. As indicated in their work, there are important assumptions associated with the approach. Bias contributions  
 374 aside, the overall level of uncertainties may be incorrect if, for example, there is significant correlation between observation  
 375 random uncertainties and random uncertainties of the background that is used in the data assimilation. A separation of scales  
 376 is indeed required in order to disentangle these two uncertainty components. Given the unique importance of radiosondes to  
 377 inform on the state of the stratosphere in a background obtained from data assimilation, such as in a reanalysis (e.g.,  
 378 Hersbach et al., 2020), there may be some components of the uncertainties (such as radiation) that are present, and possibly  
 379 correlated, in the background and the observations. For these reasons, we do not use Desroziers' diagnostics in order to  
 380 assign undisputable uncertainties to the radiosonde uncertainties. Instead, we use these diagnostics in order to detect any

381 changes in the observation uncertainties, which include instrument and representativity uncertainties, owing to the effect of  
382 balloon drift.

383

384 To this end, we run two data assimilation experiments, using a simplified data assimilation setup. Simplifications are  
385 required in order to make such an undertaking numerically affordable. Otherwise, so-called ‘full’ data assimilation  
386 experiments, using all observations at the maximum resolution, are indeed too costly to conduct, if only for such an  
387 evaluation. The simplified data assimilation setup is based on the ECMWF Integrated Forecasting System (IFS) cycle 48R1  
388 configuration (ECMWF, 2023), using an octahedral reduced Gaussian grid with 159 wavenumbers, or approximately a  
389 horizontal resolution of 69 km, instead of the ECMWF operational configuration which has a resolution of approximately 9  
390 km at present. Also, similarly for affordability reasons, the experiments only assimilate conventional observations (no  
391 satellite observations), the number of four-dimensional variational (4D-Var) minimizations is reduced from three to two, and  
392 the analysis increments are at a resolution of approximately 210 km (instead of 39 km for ECMWF operations). The  
393 simplified data assimilation setup enables us to run data assimilation experiments for a duration of two months, 01 June - 31  
394 July 1980.

395

396 The first experiment is the control. It assimilates the radiosonde observations as vertical profiles. The second experiment  
397 assimilates the radiosonde observations following the balloon trajectory when this information is available (otherwise the  
398 data are assimilated as vertical profiles). The balloon drift in the assimilation is handled by dividing the whole ascent into  
399 15-minute sub-profiles (Ingleby et al., 2018). In each sub-profile, the latitudes, longitudes, and times are invariant. In spite of  
400 this arrangement, which only partially reflects the true slanted nature of the profiles, we retain the terminology of “slanted  
401 profile” when discussing the results, for clarity within this paper.

402

403 We consider here the radiosonde observations that were assimilated in both experiments, to ensure no difference in results  
404 may be caused by sampling differences. **Table 4** shows the statistics for these data. For the reasons mentioned earlier, the  
405 interpretation of the table focuses on differences between the two experiments, and not on the absolute level of observation  
406 uncertainties determined by Desroziers’ diagnostics. Within 0.1 K, we find no detectable difference between the two  
407 experiments for the levels located below the 100 hPa pressure level. For levels located higher, i.e. pressure lower than 100  
408 hPa, one finds that background departures and estimated observation uncertainties are reduced in the experiment that  
409 assimilated the data along slanted profiles. This result is obtained for radiosondes launched from land stations as well as  
410 radiosondes launched from ships.

411

412 The differences may appear as very small and could be discarded as non important, if it was not for the fact that reducing  
413 observation and representation uncertainties is generally an impossible task, once observations were collected and processed  
414 already once. The present findings demonstrate that it is possible to generate greater return, in terms of information content,

38

39

415 through a reprocessing of the observations. The reprocessing enables here to assimilate observations along a slanted  
 416 trajectory. Furthermore, these are global statistics - see **Figure 14**. The previous sections indicated that results may vary per  
 417 launch site. Consequently, the improvements shown here, for global statistics, must hide some greater improvements at some  
 418 particular sites - see **Figure 15**.

419

420 Given previous results indicating a larger effect of the balloon drift during winter seasons (e.g. McGrath et al., 2006), and  
 421 given the much greater number of radiosonde stations in the Northern Hemisphere as compared to the Southern hemisphere  
 422 (e.g., see Figure 12), the present choice of the data assimilation season (Northern hemisphere summer, as Choi et al., 2015)  
 423 represents a conservative approach. An impact of larger magnitude may be expected at different time periods, in particular  
 424 during Northern hemisphere winter.

425

## 426 **7. Discussion and conclusions**

427 The verification and evaluation results have shown quite clearly that if at all possible, balloon displacements should be taken  
 428 into account for all relevant data assimilation applications to minimise representation errors. Ignoring the possibility to  
 429 account for observation location errors on the 100 km scale would be anachronistic, when global or regional reanalysis data  
 430 sets approach spatial resolutions finer than 20 km.

431

432 The method to reconstruct the balloon position presented in this work is limited by a few assumptions and depends on the  
 433 vertical resolution of the available profiles, and the conformance of the weather balloons to modern ascent speeds. For the  
 434 applications tested, an attempt was made to obtain the best results globally, and a clear positive impact was found,  
 435 particularly when comparing to ERA5 in the early 2000s, although positive results were also found at other times (e.g.,  
 436 1980s). This is also consistent with other findings in similar settings where trajectory data are used to reduce representation  
 437 errors (e.g., Laroche and Sarrazin, 2013).

438

439 The data assimilation experimental setup employed here is a simplified one, as compared to what may be used in a present-  
 440 day reanalysis configuration such as ERA5. Yet, we observe a positive impact of the balloon drift in terms of reducing the  
 441 background departures and the observation uncertainty, using Desroziers' diagnostics, for temperatures in the stratosphere.  
 442 We expect that the quality of the corrections made to use radiosondes at a displaced horizontal position, as compared to  
 443 using them at a vertical position, would increase when the background resolution and/or the background quality is increased.  
 444 In addition, assessing the impact of the balloon drift sensitivity to the assimilation of other observations alongside  
 445 radiosondes would be worth analysing. However, owing to time and computational constraints, it was not possible to

446 investigate further these effects with full data assimilation experiments at higher horizontal resolution and using all available  
447 information, but we note this would be a useful pursuit.

448

449 The results of the tests have shown that the method is successful in reconstructing displacements and improving the accuracy  
450 of the atmospheric data. Whilst the additional information provided by the method may not always be a visible improvement  
451 for individual comparisons, it is of significant value when the displacement changes the gridbox of the model being  
452 compared. This has been demonstrated by improved means in the plots and better agreement between observations and  
453 ERA5.

454

455 The value of improving radiosonde observations by reprocessing of the positions was evaluated by conducting reduced-  
456 resolution data assimilation experiments, covering a two-month period in summer 1980. In the future, it would be desirable  
457 that the impact of similar activities that seek to improve the observational record be more regularly evaluated in the  
458 generation of downstream climate products. Such an evaluation should consider a longer time period and include the impact  
459 on low-frequency variability in the products. For products such as reanalyses, obtained via data assimilation, this should  
460 entail full-resolution Observing System Experiments (OSEs). For other types of climate products, including those powered  
461 by new opportunities such as Artificial Intelligence or Machine Learning (e.g., Singh et al., 2022), it is important that  
462 mechanisms be found to evaluate the impact of using the observations and how changes made in their handling affects the  
463 outcome.

464

465 Further experimentation using observation data from the period 2000 - 2020 is crucial and is likely to produce more  
466 compelling outcomes. The effective use of this method for informing future climate reanalysis is one of the main objectives.  
467 As the world faces increasing challenges related to climate change, the importance of accurate atmospheric data and the  
468 potential of new methods to improve it cannot be overstated. The use of improved position metadata with radiosonde  
469 observations can account for previously unexplainable phenomena, demonstrating the potential of this method to shed new  
470 light on atmospheric data analysis. In addition, the method has the potential to improve the accuracy of reanalyses and  
471 climate predictions, which are crucial for many socio-economic sectors.

472

473 To achieve the optimal representation of the data, precise details regarding time and location must be available for every  
474 observation. One significant issue concerns the TAC format's transmission and storage of data, which often only includes a  
475 nominal timestamp such as 00:00 UTC or 12:00 UTC. However, the actual launch of the respective balloon in most cases  
476 took place 30-60 minutes earlier. The precise time difference from the nominal time is frequently unknown, therefore  
477 displacement information cannot be utilised to its fullest extent. Since temperature can vary by more than 1 K/hour in the  
478 boundary layer just due to the diurnal cycle this issue should be addressed. There are well known examples where changes in  
479 the sampling of the diurnal cycle introduced spurious trends into climate data products (Mears and Wentz, 2005). Whenever

44

45

480 possible, the precise launch time should be used. In cases where this information is not available for individual ascents, the  
481 time difference between the nominal and actual launch can often be determined from earlier or later ascents. Operators are  
482 normally advised to minimise the variation throughout the launch procedure and, therefore, launch balloon sondes at the  
483 same time every day.

484

485 Additional work to better understand the causes of variation in balloon ascent speeds (e.g., Zhang et al., 2019) could help  
486 further improve the results. Also, given all the uncertainty sources, it could be possible to generate an ensemble of  
487 trajectories for each ascent. Pendulum motion is an effect that would need to be better understood, as it could be of  
488 importance for example in geographical locations where wind advection leads to small horizontal displacements.

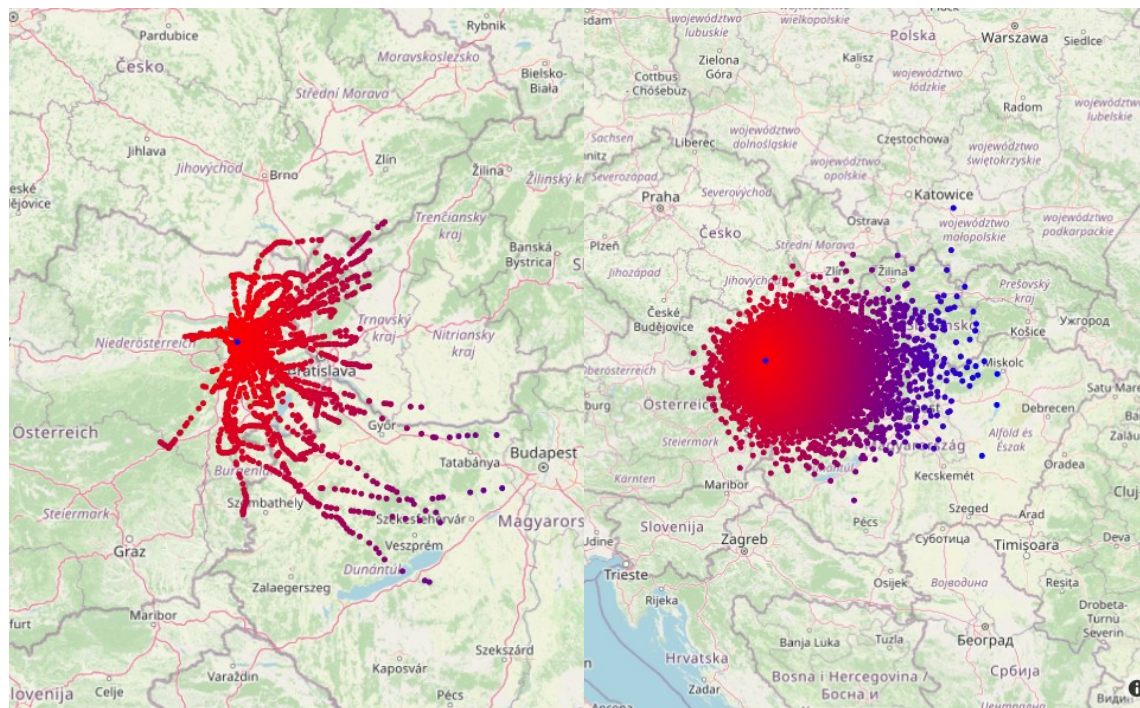
489 |

490 | The same approach as presented in this paper can be used to reprocess rocketsondes, or dropsondes, ozonesondes, or any  
491 other in-situ sonde carried advected by the wind, provided the necessary information is available. Taking into account the  
492 accurate balloon position would also be beneficial when comparing radiosonde observations with GNSS radio occultation  
493 (RO) observations (Gilpin et al. 2018). Indeed, while it is established practice to consider the tangent point drift slanted  
494 profile of the RO data is considered (e.g., Poli and Joiner, 2004), radiosonde data is frequently presumed to move vertically  
495 only.

496

497 In conclusion, the development and testing of the method for reconstructing displacements based on the wind profile shows  
498 promising results. The results presented in this paper suggest taking balloon displacements into account when producing  
499 meteorological or climatological data based on upper-air in situ balloon-borne observations.

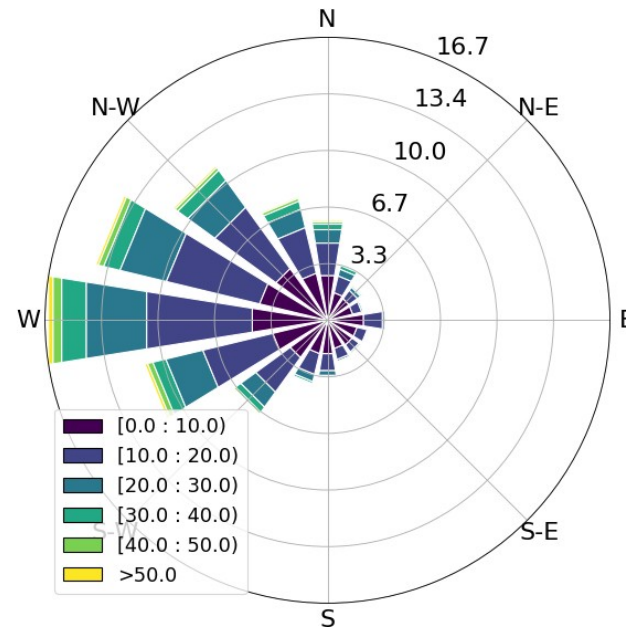
## 501 Appendices



502

503

© OpenStreetMap contributors 2023. Distributed under the Open Data Commons Open Database License (ODbL) v1.0.



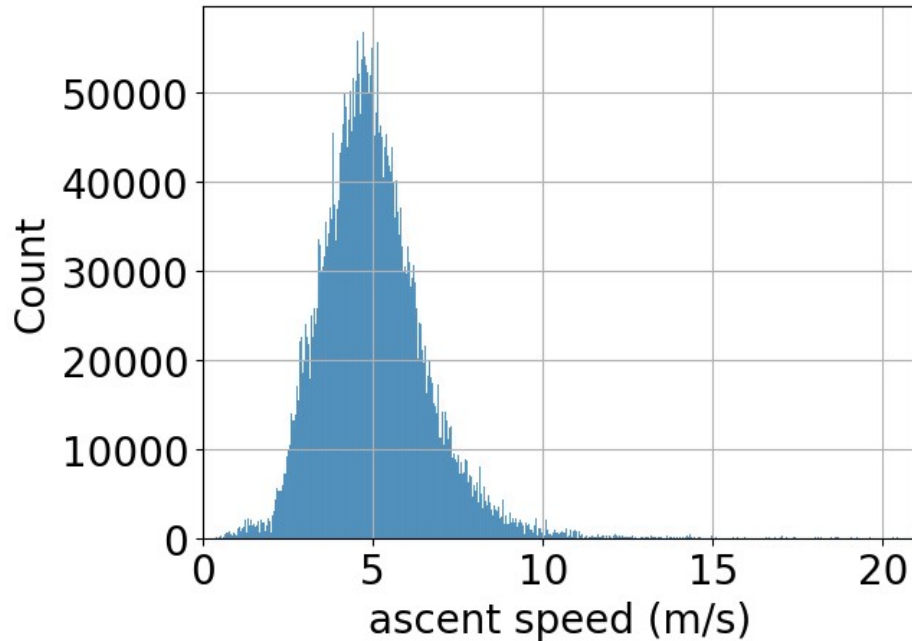
504

50

51

505 Figure 1: Upper panels: **Balloon displacements for station Vienna Hohe Warte, Austria (WIGOS ID 0-20001-0-11035)**. Central  
 506 blue dot denotes station location, , central blue dot) other dots are balloon positions calculated from wind data as explained  
 507 in text, coloured red to blue with increasing distance. Note the area covered is non-isotropic around the launch site. Left panel:  
 508 Trajectories of all radiosonde ascents during the year 2000. Right panel – maximum displacements of all available ascents for all  
 509 years between 1950 and 2021. Lower panel: windrose of Vienna Hohe Warte station for all available wind data. Colour indicates  
 510 wind speed [m/s], radius indicates frequency distribution [%] of direction, from where the wind comes from (sectors) and wind  
 511 speed (colors). [Displacements are based on the the IGRA dataset and calculated via the method introduced in Section 2.3.](#)

512 |



513

514 Figure 2: The observed ascent speeds from a sample of approximately 10 million BUFR encoded observations with known altitude  
 515 time series in 2020.

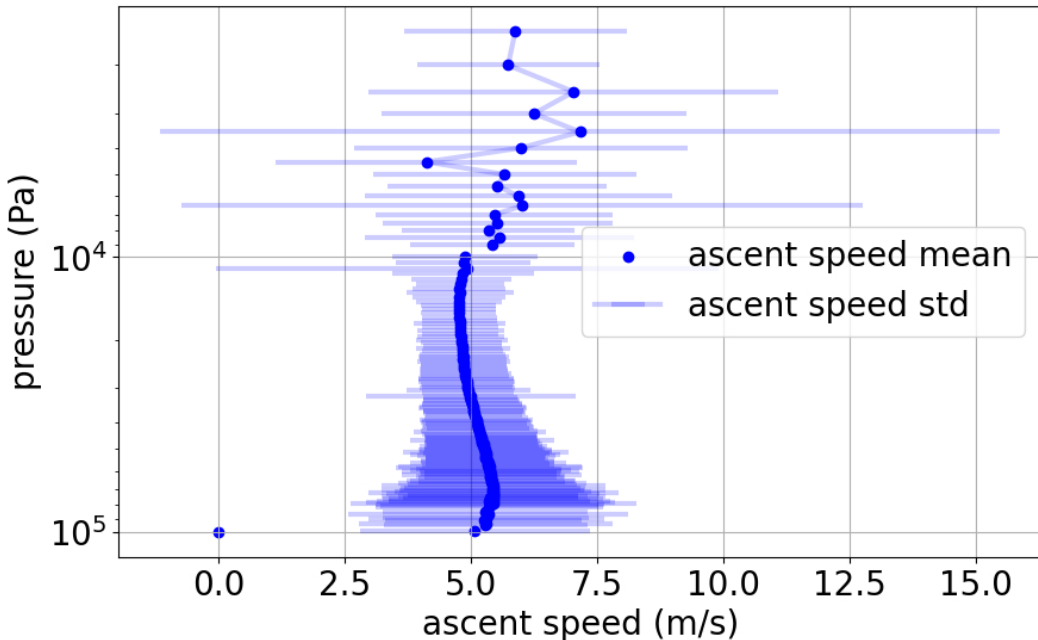
516  
517  
518

Figure 3: Mean ascent speed with standard deviation bars for all radiosonde ascents from Riverton USA, in 2020, derived from high resolution BUFR data.

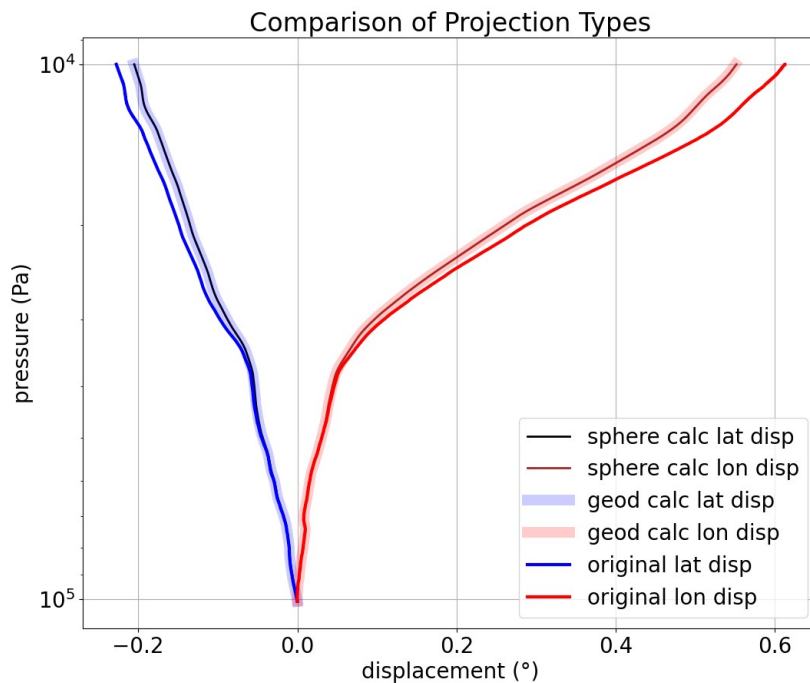
519  
520  
521  
522

Figure 4: Calculated displacements (black and brown for spherical earth, thick light blue and red for WGS84). Observed displacements stored in BUFR displacements (blue and red) are included for comparison. Tallahassee, Florida - USA 2020.05.31 23:19:00

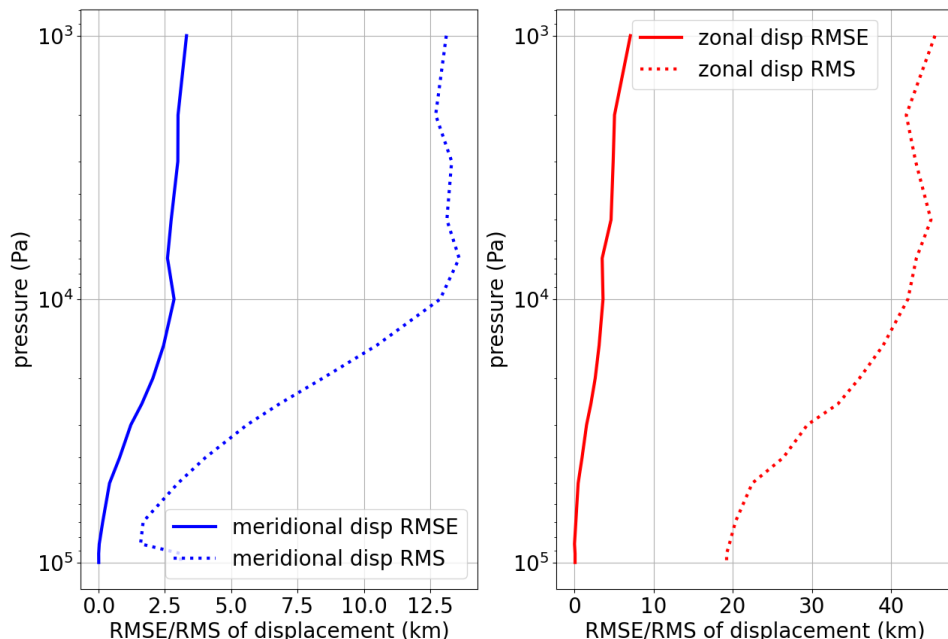


Figure 5: RMS of meridional (blue dotted) and zonal (red dotted) displacements and RMSE between observed (from GPS) and modelled displacements (solid blue and solid red, respectively). The samples contain all BUFR encoded ascents in the summer months of 2020 (more than 10000).

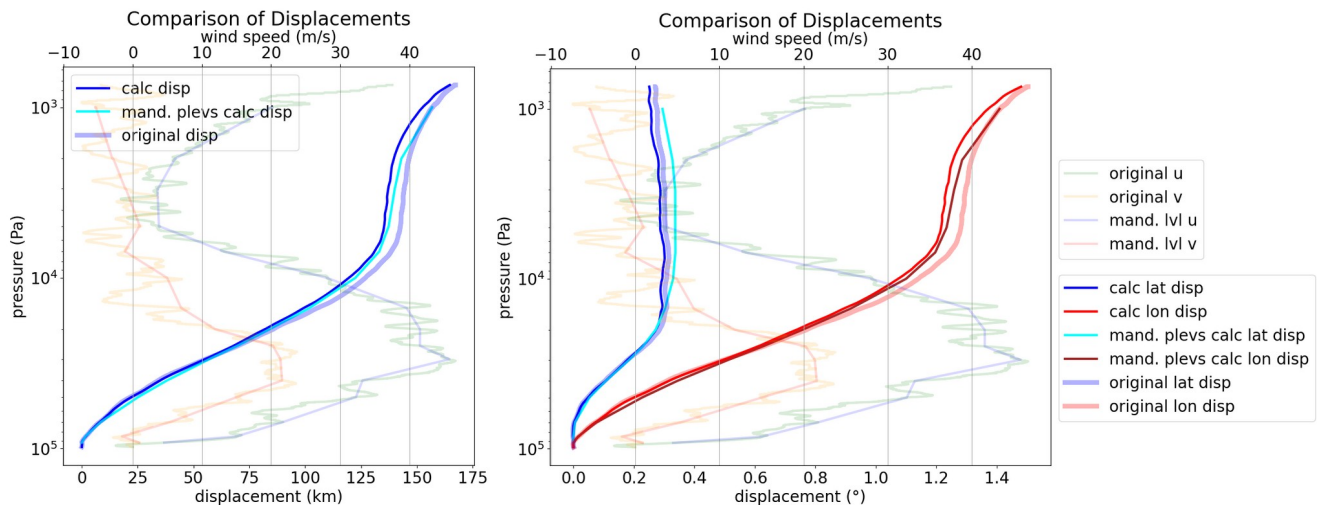
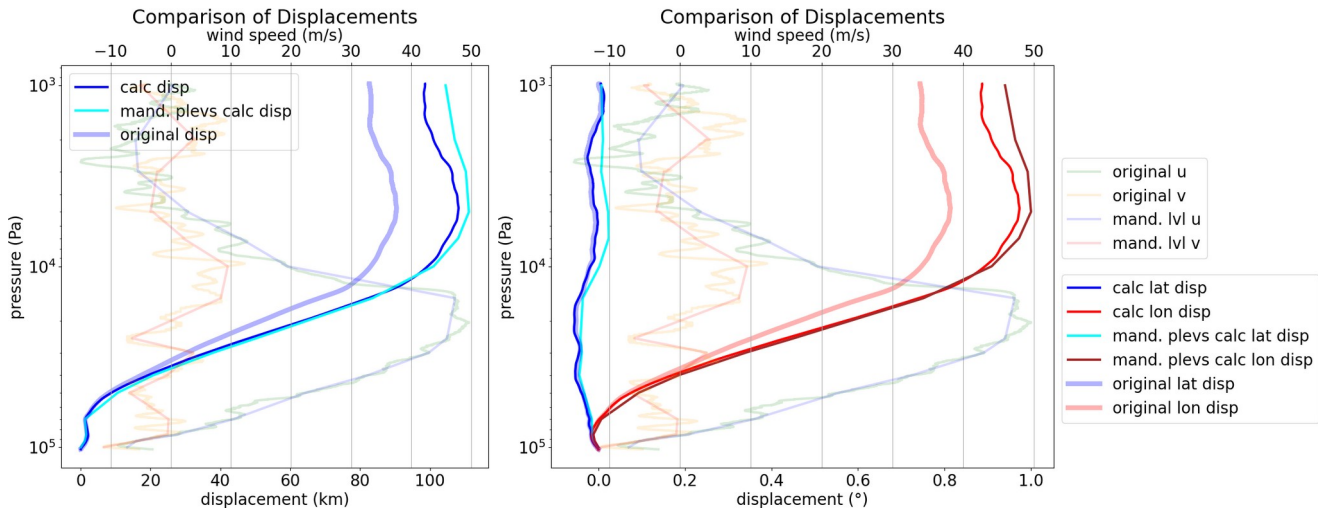


Figure 6: Vertical profiles of displacements (starting at zero at surface), calculated from observed winds (thin lines) or taken from BUFR thick light lines. The profiles of observed wind (thin light colors) are plotted to the upper x axis - Peachtree City, Georgia - USA 31.01.2021 23:24:00. Left panel: overall displacements in km, right panel: lat and lon displacements in degrees as encoded in BUFR.

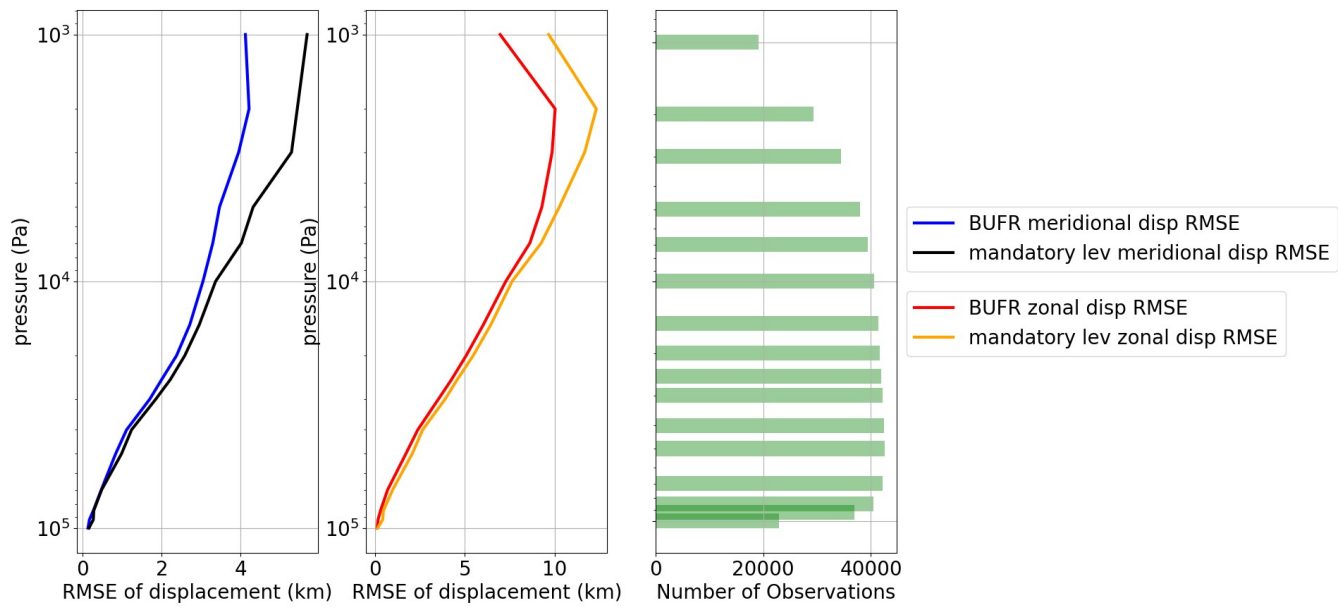


534  
535  
536  
537  
538

Figure 7: Vertical profiles of displacements (starting at zero at surface), calculated from observed winds (thin lines) or taken from BUFR thick light lines. The profiles of observed wind (thin light colors) are plotted to the upper x axis - Ishigaki, Okinawa - Japan 2019.12.31 23:31:00 . Left panel: overall displacements in km, right panel: lat and lon displacements in degrees as encoded in BUFR.

539  
540  
541

542



543

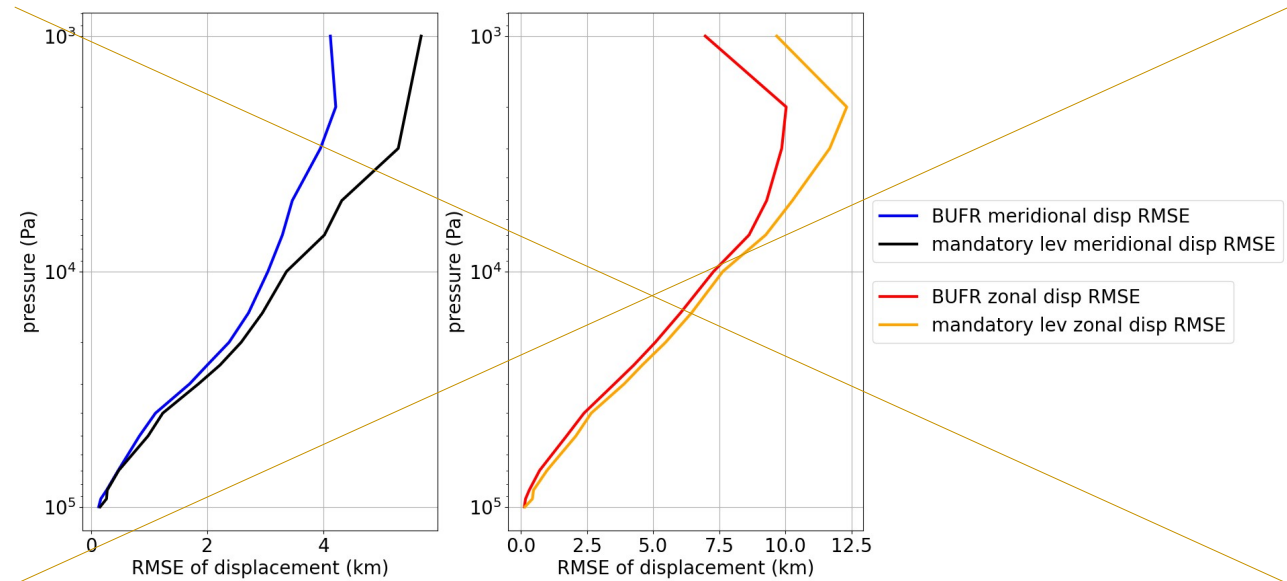
544

545

546

547

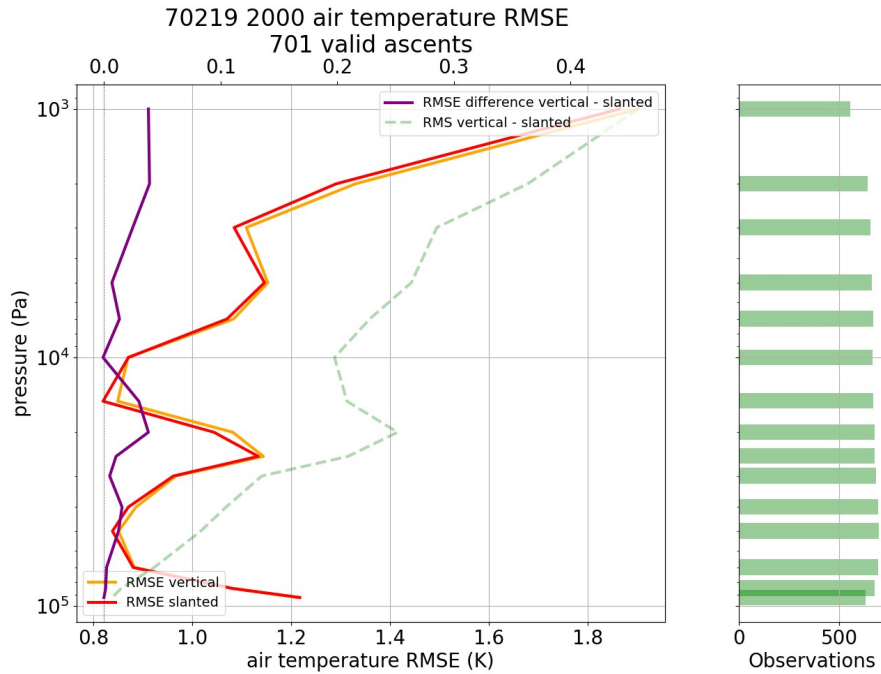
548



**Figure 8: RMSE between observed and modelled displacements of meridional (left panel) and zonal (right panel) components, averaged over all stations available in October 2014, one of the first months with a sizable number of high-resolution BUFR encoded profiles. Blue and red are RMSE profiles obtained by using the full vertical resolution of BUFR observations, black and orange are RMSE profiles, and obtained by using only mandatory level information.**

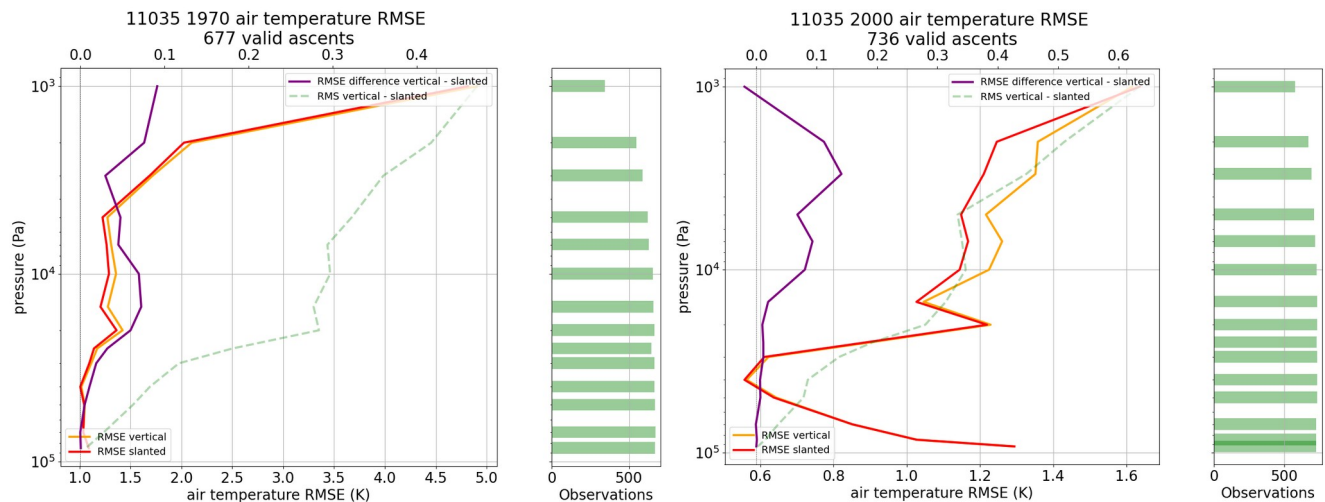
65

66



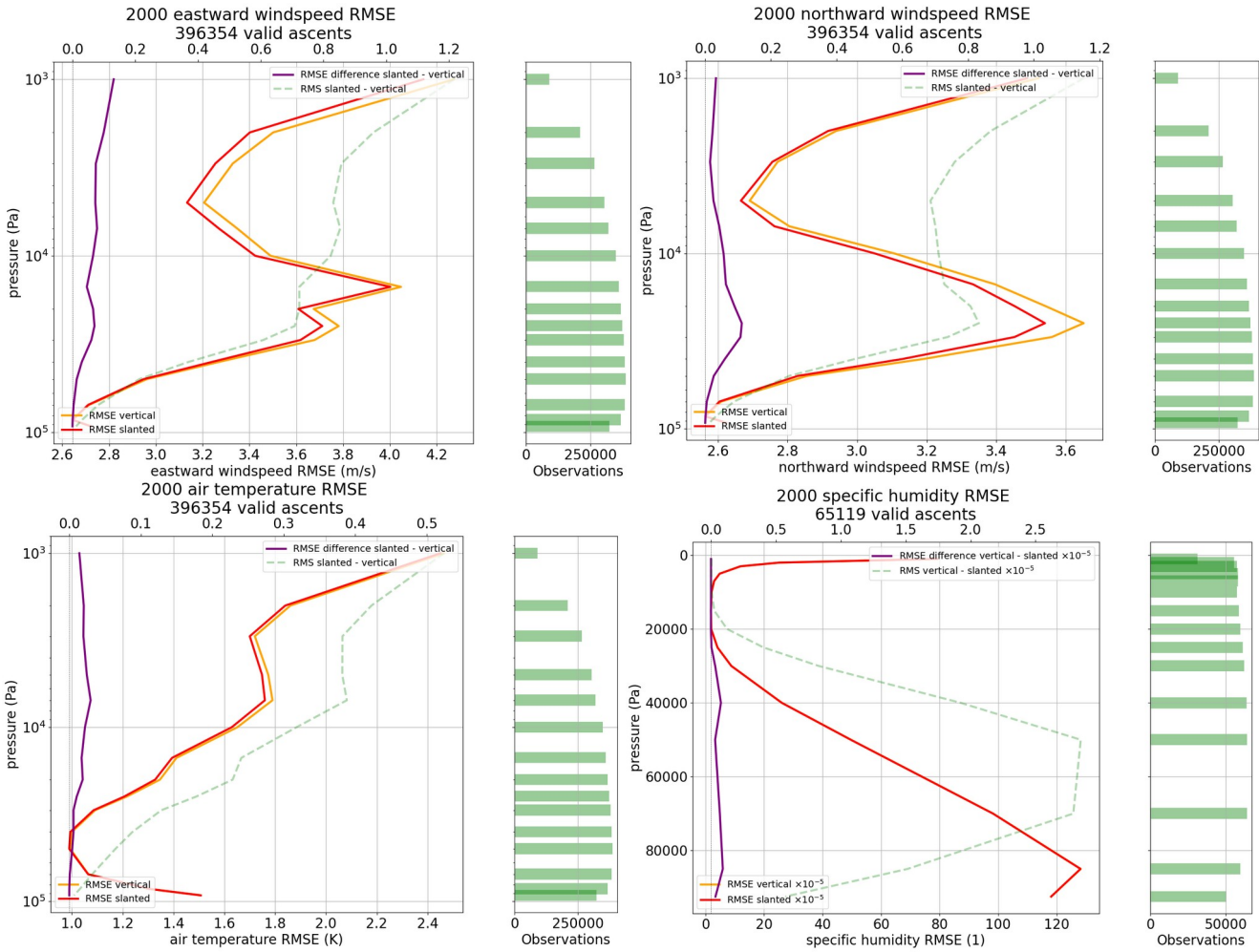
549  
550  
551  
552  
553  
554

Figure 9: Bethel Airport, Alaska all 2020 ascents. RMSE (obs - ERA5) of base coordinate temperatures minus sonde temperatures (orange) and RMSE (obs - ERA5) of displaced temperatures minus sonde temperatures (red), also RMS of displaced minus base (green dashed) to show the magnitude of difference between base and displaced temperatures. Positive difference between orange and red graphs (purple line, upper x axis) shows improvement due to more accurate balloon position. Green bars on the right indicate sample sizes at different levels.

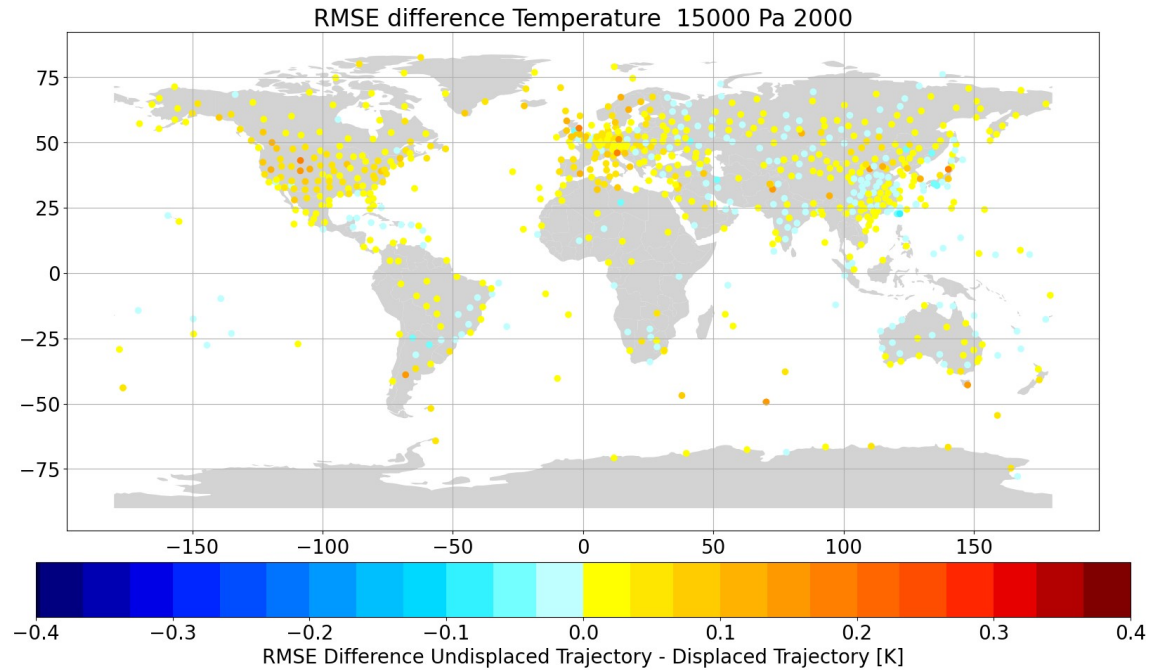


555  
556  
557  
558  
559  
560

Figure 10: Vienna Hohe Warte, Austria - Left: 1970 all ascents, Right: 2020 all ascents. Different x-axes scales are used. RMSE (obs - ERA5) of vertical temperature minus sonde of temperature assuming vertical ascents (orange, lower x-axis) and RMSE (obs - ERA5) of slanted temperature from slanted ascents, taking balloon drift into account minus sonde temperature (red, lower x-axis). Positive difference between orange and red graphs (purple line, upper x axis) shows improvement due to more accurate balloon position.

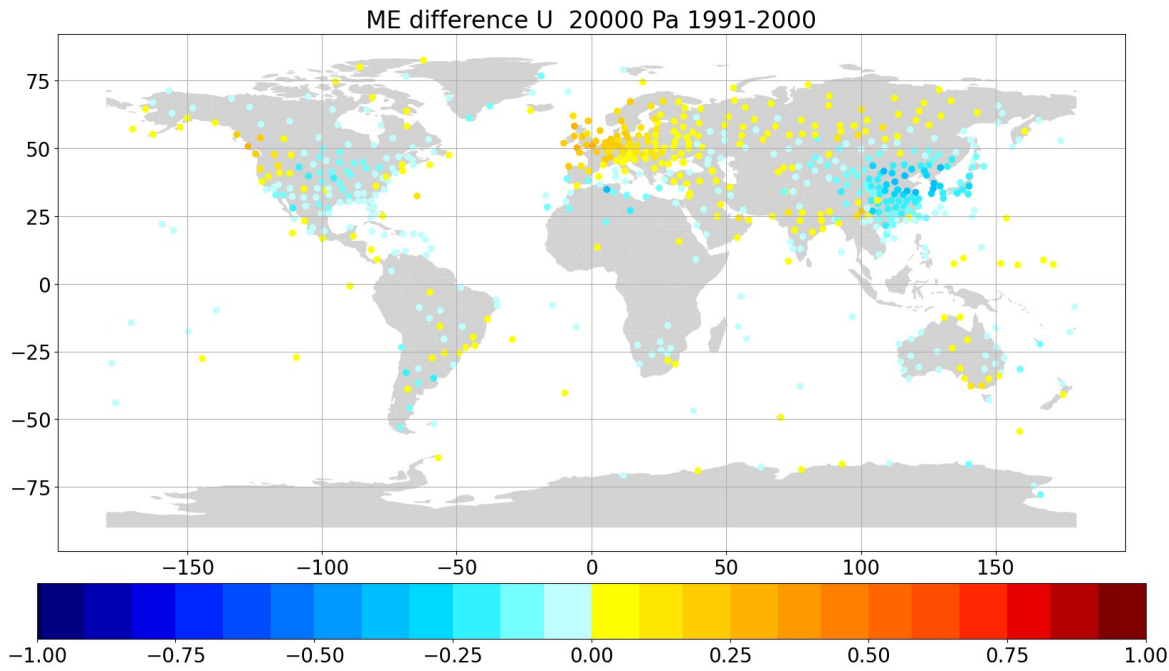


561  
562  
563  
564 **Figure 11: Global RMSE (obs - ERA5 background) assuming vertical ascents (orange) and RMSE (obs - ERA5 background) from**  
565 **reconstructed slanted ascents (red), calculated from all available ascents of year 2000. The differences between orange and red**  
566 **graphs (purple line, upper x axis) shows how much the better balloon position improved the temperature data (positive =**  
567 **improvement). The “RMS vertical - slanted” (green dashed line, upper x axis) indicates how much the ERA5 background varies**  
568 **on average between the vertical and slanted balloon profiles. - Top left: u wind component; Top right: v wind component; Bottom**  
569 **left: temperature; Bottom right: specific humidity in kg/kg (note scaling factor  $10^{-5}$ ).**



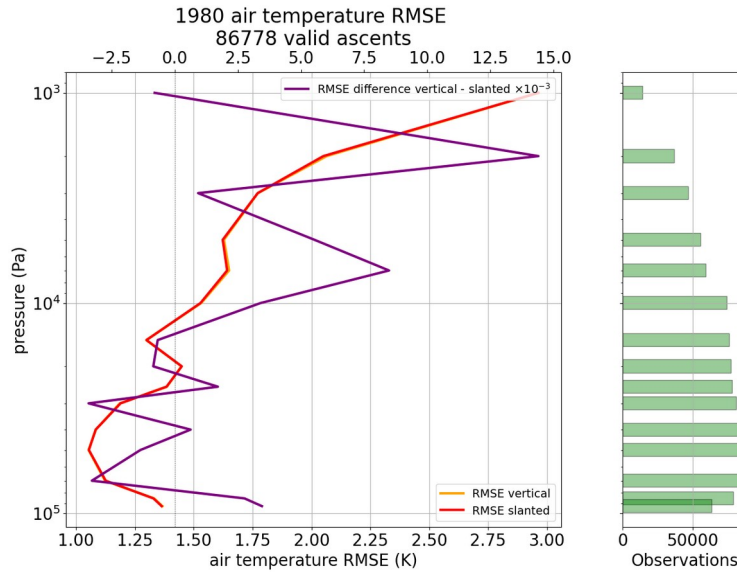
571  
572  
573  
574  
575

Figure 12: Global stations difference of temperature [K] observation RMSE (obs - ERA5) when compared to background at station coordinates minus the temperature observation RMSE (obs - ERA5) when compared to background at displaced position - Positive values indicate improvement due to more accurate balloon position. All available observations at 150 hPa averaged over all ascents in the year 2000.



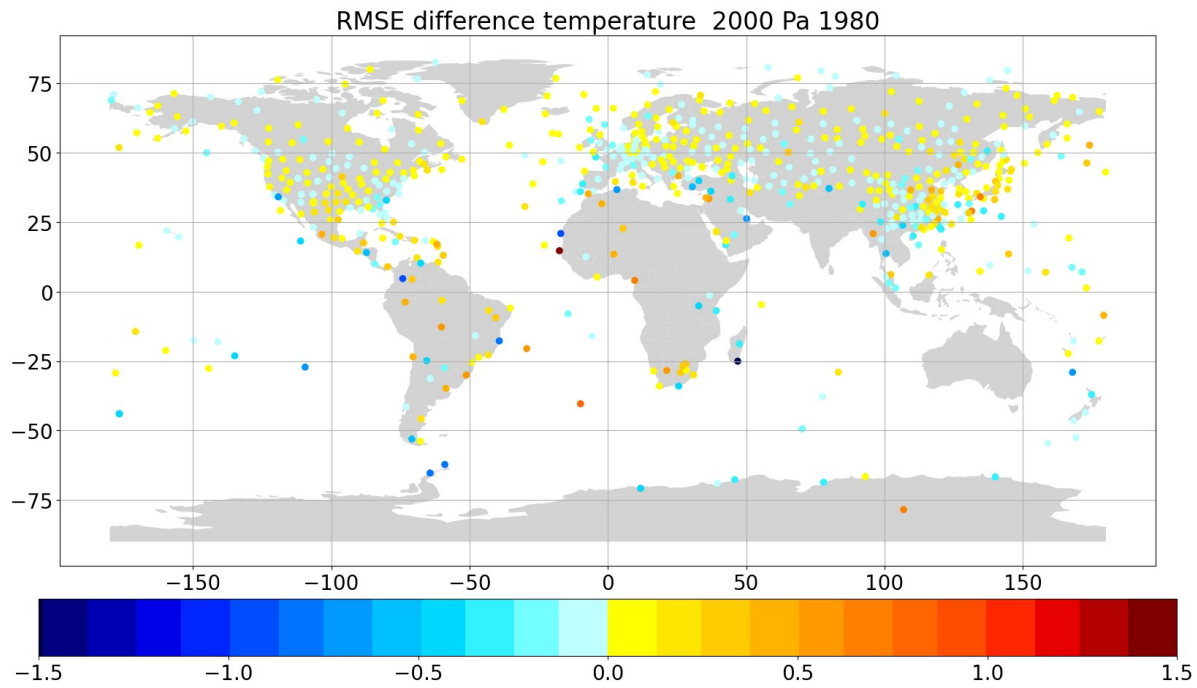
576  
577  
578

Figure 13: Mean zonal (u) wind [m/s] difference obs - ERA5 background at station position minus obs - ERA5 background at displaced position. All available values on 200 hPa of years 1991 - 2000.



579

580 **Figure 14:** Air temperature obs-bg RMSE difference for experiment “vertical” (orange) and for experiment “slanted” (red). The  
 581 difference of differences (orange-red) yields the purple line, upper x axis, note scaling factor  $10^{-3}$ . Positive values indicate  
 582 improvement due to more accurate balloon position. All available stations on mandatory pressure levels between 1980.06.01-  
 583 1980.07.31.



584

585 **Figure 15:** Air temperature obs-bg RMSE [K] difference of experiment “vertical” minus RMSE of experiment “slanted”. Positive  
 586 values indicate improvement due to usage of more accurate balloon position. All available stations on 20 hPa between 1980.06.01-  
 587 1980.07.31.

588 **Table 1 3: Ascent speed percentiles for a sample of 10.000.000 observations with known altitude time series in 2020.**

Percentile	Value	Unit
1	2.05	[m/s]
5	2.82	[m/s]
25	4.01	[m/s]
75	5.85	[m/s]
95	7.74	[m/s]
99	10.09	[m/s]

589

591 **Formula 1, 2: Calculation of the vertical gradient of temperature.** See Table 21.

592 
$$\Gamma_{(p)} = \frac{\delta T}{\delta z} = \frac{\delta T}{\delta p} \frac{\delta p}{\delta z} = \frac{-\delta T}{\delta p^\kappa} \frac{\delta p^\kappa}{\delta p} \frac{\delta p}{\delta z} \quad (1)$$

593 
$$\Gamma_{(p)} = \frac{-\delta T}{\delta p^\kappa} \frac{p^\kappa}{T} \frac{\kappa g}{R_d} \quad (2)$$

594

595

596 **Formula 3: Calculation of layer height.** See Table 2 1.

597 
$$\Delta z_{(i \rightarrow i+1)} = \frac{T_i}{\Gamma_i} \left( \frac{p_{i+1}}{p_i} \right)^{\frac{-\Gamma_i R_d - 1}{g}} \quad (3)$$

598

599

600

601 **Table 21: Height profile calculation. Explanation of all used variables.**

Symbol	Description	Unit	Data source
$\Gamma$	temperature lapse rate	[K/m]	observed variable
p	pressure	[Pa]	observed variable
T	temperature	[K]	observed variable
$\Delta z$	layer height	[m]	calculated variable
$\kappa$	isentropic expansion factor	[1]	$\kappa = R/cp$
$c_p$	specific heat capacity of air at constant pressure	[J/kg/K]	constant (1005.7)
$R_d$	gas constant for dry air	[J/kg/K]	constant (286.7)
g	standard gravity	[m/s <sup>2</sup> ]	constant (9.80665)

602

603

604 **Formula 4: Transport of the balloon with the wind. See Table 32.**

$$605 \quad \vec{s}_{(i+1)} = \frac{\vec{u}_{(i \rightarrow i+1)} * \Delta z_{(i \rightarrow i+1)}}{w_{balloon}} \quad (4)$$

606

607

608 **Table 32: Time interval calculation. Explanation of all used variables.**

Symbol	Description	Unit	Data source
$\vec{s}$	distance travelled	[m]	0 at i = 0, lon for u, lat for v
$\vec{u}$	wind	[m/s]	observed variable, u and v components of wind
$\Delta z$	layer height	[m]	calculated variable
w	rate of ascension	[m/s]	5, prescribed variable

609

611 **Table 4: Statistics for the radiosonde observations actively used by both data assimilation experiments (vertical and slanted),**  
 612 **separating between radiosondes launched from land stations and radiosondes launched from ships. P indicates the pressure (hPa),**  
 613 **RSD indicates the robust standard deviation of background departures (i.e., before assimilation), SIGO indicates the estimated**  
 614 **observation uncertainty (see text for details), and N indicates the data count. Results that differ between the two experiments are**  
 615 **shown in bold and underlined. Observations that were used by only either one of the two experiments are excluded from these**  
 616 **statistics.**

Pressure level range	$P \geq 500 \text{ hPa}$		$500 \text{ hPa} > P \geq 100 \text{ hPa}$		$100 \text{ hPa} > P \geq 1 \text{ hPa}$	
Experiment	Vertical	Slanted	Vertical	Slanted	Vertical	Slanted
<b>Radiosondes from land stations</b>						
<b>RSD</b>	1.2 K	1.2 K	1.3 K	1.3 K	<b><u>2.1 K</u></b>	<b><u>2.0 K</u></b>
<b>SIGO</b>	1.1 K	1.1 K	1.2 K	1.2 K	<b><u>2.1 K</u></b>	<b><u>2.0 K</u></b>
<b>N</b>	31,027,909	31,027,909	30,229,363	30,229,363	1,358,298	1,358,298
<b>Radiosondes from ships</b>						
<b>RSD</b>	1.2 K	1.2 K	1.2 K	1.2 K	<b><u>1.6 K</u></b>	<b><u>1.5 K</u></b>
<b>SIGO</b>	1.1 K	1.1 K	1.2 K	1.2 K	<b><u>1.8 K</u></b>	<b><u>1.6 K</u></b>
<b>N</b>	838,265	838,265	669,655	669,655	34,709	34,709

620 **Code and data availability**

621 Radiosonde data used in the present work are available from <https://doi.org/10.7289/V5X63K0Q> (IGRA) and  
 622 <https://doi.org/10.24381/cds.f101d0bf> (C3S CDS) and the National Centers for Environmental Information (NOAA NCEI)  
 623 Radiosonde Archive (<https://www.ncei.noaa.gov/data/ecmwf-global-upper-air-bufr/archive/>). Climate reanalysis data  
 624 (ERA5) are available from <https://doi.org/10.24381/cds.bd0915c6>. The code discussed in this paper is available from  
 625 <https://doi.org/10.5281/zenodo.10663306>.

626 **Author contribution**

627 Ulrich Voggenberger and Leopold Haimberger designed the method to estimate balloon positions. Ulrich Voggenberger  
 628 developed the code and optimised the estimations and calculations with further input from Federico Ambrogi. Ulrich  
 629 Leopold Haimberger and Ulrich Voggenberger validated and evaluated the results based on ERA5 data. Paul Poli ran the  
 630 data assimilation experiments and evaluated the results in section 6. Ulrich Voggenberger prepared the manuscript with  
 631 contributions from all co-authors.

632 **Competing interests**

633 The contact author has declared that none of the authors has any competing interests.

634 **References**

635 Aberson, S. D., Sellwood, K. J., & Leighton, P. A.: Calculating Dropwindsonde Location and Time from TEMP-  
 636 DROP Messages for Accurate Assimilation and Analysis. In *Journal of Atmospheric and Oceanic Technology* (Vol.  
 637 34, Issue 8, pp. 1673–1678). American Meteorological Society. <https://doi.org/10.1175/jtech-d-17-0023.1>, 2017.

638 Alexander, P., and dDe La Torre, A.: Uncertainties in the measurement of the atmospheric velocity due to balloon-  
 639 gondola pendulum-like motions. *Adv. Space Res.*, 47 (4):736-739, <https://doi.org/10.1016/j.asr.2010.09.020>, 2011.

640 Choi, Y., J. Ha, and G. Lim: Investigation of the Effects of Considering Balloon Drift Information on Radiosonde  
 641 Data Assimilation Using the Four-Dimensional Variational Method. *Wea. Forecasting*, 30, 809–826,  
 642 <https://doi.org/10.1175/WAF-D-14-00161.1>, 2015

643 Crutcher, H. L.,: Distribution of radiosonde errors. NOAA Tech. Rep. Environmental Data and Information Service  
 644 (EDIS), 32, [https://repository.library.noaa.gov/view/noaa/30830/noaa\\_30830\\_DS1.pdf](https://repository.library.noaa.gov/view/noaa/30830/noaa_30830_DS1.pdf), 1979.

645 Dabberdt, W. F., and Turtiainen, H.: Observations platforms: Radiosondes, in Encyclopedia of Atmospheric Sciences  
 646 (Second Edition), eds. G. R. North, J. Pyle, F. Zhang, Academic Press, pp 273-284, ISBN 9780123822253.  
 647 <https://www.sciencedirect.com/referencework/9780123822253/encyclopedia-of-atmospheric-sciences>, 2015.

648 Desroziers, G., Berre L., Chapnik B., and Poli, P.: Diagnosis of Observation, Background and Analysis-Error  
 649 Statistics in Observation Space. Quarterly Journal of the Royal Meteorological Society 131, no. 613 (October 1,  
 650 2005): 3385–96. <https://doi.org/10.1256/qj.05.108>., 2005.

651 Durre, I., Yin, X., Vose, R. S., Applequist, S., Arnfield, J., Korzeniewski, B., and Hundermark, B.: Integrated Global  
 652 Radiosonde Archive (IGRA), Version 2. NOAA National Centers for Environmental Information. HYPERLINK  
 653 "https://doi.org/10.7289/V5X63K0Q" <https://doi.org/10.7289/V5X63K0Q>, 2016.

654 Durre, I., X. Yin, R. S. Vose, S. Applequist, and J. Arnfield, 2018: Enhancing the Data Coverage in the Integrated  
 655 Global Radiosonde Archive. J. Atmos. Oceanic Technol., 35, 1753–1770, HYPERLINK  
 656 "https://doi.org/10.1175/JTECH-D-17-0223.1" <https://doi.org/10.1175/JTECH-D-17-0223.1>.

657 Dutton, J. A.: The ceaseless wind: An Introduction to the Theory of Atmospheric Motion. Dover Publications, New-  
 658 York, 617 pp., ISBN:978-0486495033, <https://doi.org/10.1029/88EO01137>, 1986.

659 ECMWF: IFS Documentation CY48R1. <https://www.ecmwf.int/en/publications/ifs-documentation>, last access 25 Oct  
 660 2023

661 Favà, V., Curto, J. J., and Gilabert, A.: Thermodynamic model for a pilot balloon, Atmos. Meas. Tech. [preprint],  
 662 <https://doi.org/10.5194/amt-2021-206>., 2021.

663 Gilpin, S., Rieckh, T., and Anthes, R.: Reducing representativeness and sampling errors in radio occultation-  
 664 radiosonde comparisons, Atmos. Meas. Tech., 11, 2567–2582, <https://doi.org/10.5194/amt-11-2567-2018>, 2018.

665 Hersbach, H, Bell, B, Berrisford, P, et al.: The ERA5 global reanalysis. Q J R Meteorol Soc. 146: 1999–2049.  
 666 HYPERLINK "https://doi.org/10.1002/qj.3803" <https://doi.org/10.1002/qj.3803>, 2020.

667 Hersbach, H., Bell, B., Berrisford, P., et al.: Characteristics of ERA5 and innovations for ERA6. Copernicus Climate  
 668 Change Service General Assembly 2022. Available from HYPERLINK  
 669 "https://climate.copernicus.eu/sites/default/files/2022-09/S3\_Hans\_Hersbach\_v1.pdf" [https://climate.copernicus.eu/sites/default/files/2022-09/S3\\_Hans\\_Hersbach\\_v1.pdf](https://climate.copernicus.eu/sites/default/files/2022-09/S3_Hans_Hersbach_v1.pdf), last accessed 26-03-2023.

670 ICAO Standard Atmosphere - ISA <https://www.foehnwall.at/meteo/isa.html>, last access 25-10-2023.

671 Ingleby, B., P. Pauley, A. Kats, J. Ator, D. Keyser, A. Doerenbecher, E. Fucile, J. Hasegawa, E. Toyoda, T. Kleinert,  
 672 W. Qu, J. St James, W. Tennant, and R. Weedon,: Progress toward High-Resolution, Real-Time Radiosonde Reports.  
 673 Bull. Amer. Meteor. Soc., 97, 2149-2161, <https://doi.org/10.1175/BAMS-D-15-00169.1>. 2016.

674 Ingleby, B., Isaksen, L., Kral, T., Haiden, Th., and Dahoui, M.: Improved use of atmospheric in situ data. ECMWF  
 675 Newsletter 155. <https://doi.org/10.21957/cf724bi05s>, 2018.

677 Ingleby, B., Motl, M., Marlton, G., Edwards, D., Sommer, M., von Rohden, C., Vömel, H., and Jauhainen, H.: On  
 678 the quality of RS41 radiosonde descent data, *Atmos. Meas. Tech.*, 15, 165–183, <https://doi.org/10.5194/amt-15-165-2022>, 2022.

679

680 Kats A., Balagourov A & Grinchenko V. (2005) The impact of new RF95 radiosonde, introduction on upper-air data  
 681 quality in the North-west region of Russia. Poster Pw(07), TECO-2005, WMO/TD- No. 1265; IOM Report- No. 82.

682 Keyser, D., 2000: RAOB/PIBAL Balloon Drift Latitude, Longitude, & Time Calculation In PREPBUFR. Available  
 683 from [HYPERLINK](https://www.emc.ncep.noaa.gov/mmb/data_processing/prepbufr.doc/balloon_drift_for_TPB.htm)  
 684 "https://www.emc.ncep.noaa.gov/mmb/data\_processing/prepbufr.doc/balloon\_drift\_for\_TPB.htm" https://  
 685 www.emc.ncep.noaa.gov/mmb/data\_processing/prepbufr.doc/balloon\_drift\_for\_TPB.htm [Last accessed 26-03-2023]

686 Kitchen, M.: Representativeness errors for radiosonde observations. *Q. J. R. Meteorol. Soc.*, 115: 673-700.  
 687 <https://doi.org/10.1002/qj.49711548713>, 1989.

688 Laroche, S., and Sarrazin, R.: Impact of Radiosonde Balloon Drift on Numerical Weather Prediction and Verification.  
 689 *Weather and Forecasting*, 28 (3), 772–782. <https://doi.org/10.1175/waf-d-12-00114.1>, 2013.

690 McGrath, R., T. Semmler, C. Sweeney, and S. Wang,: Impact of balloon drift errors in radiosonde data on climate  
 691 statistics. *J. Climate*, 19, 3430–3442, <https://doi.org/10.1175/JCLI3804.1>, 2006.

692 Mears, C. A., and Wentz, F. J.: The effect of diurnal correction on the satellite-derived lower tropospheric  
 693 temperature. *Science*, 309, 1548–1551. <https://doi.org/10.1126/science.1114772>, 2005.

694 Murillo, J., Mejia, J., Galvez, J., Orozco, R., and Douglas, M.: Quality control of pilot balloon network data for  
 695 climate monitoring. *Amer. Meterol. Soc. 15th Conf. Appl. Clim., 13th Symp. Meteorol. Obs. Instr.*, **JP1.30.**,  
 696 <https://api.semanticscholar.org/CorpusID:56365106>, 2005.

697 OpenStreetMap: OpenStreetMap® is open data, licensed under the Open Data Commons Open Database License  
 698 (ODbL) by the OpenStreetMap Foundation (OSMF). You are free to copy, distribute, transmit and adapt our data, as  
 699 long as you credit OpenStreetMap and its contributors. If you alter or build upon our data, you may distribute the  
 700 result only under the same licence. The full legal code explains your rights and responsibilities. Our documentation is  
 701 licensed under the Creative Commons Attribution-ShareAlike 2.0 license (CC BY-SA 2.0). Available from  
 702 [HYPERLINK](https://planet.openstreetmap.org) "https://planet.openstreetmap.org" https://planet.openstreetmap.org, 2023.

703 Poli, P., and Joiner, J.: Effects of horizontal gradients on GPS radio occultation observation operators. I: Ray tracing.  
 704 Q.J.R. Meteorol. Soc., 130: 2787-2805. [HYPERLINK](https://doi.org/10.1256/qj.03.228)  
 705 "https://doi.org/10.1256/qj.03.228" https://doi.org/10.1256/qj.03.228, 2004.

706 Seidel, D. J., Sun, B., Pettey, M., and Reale, A.: Global radiosonde balloon drift statistics, *J. Geophys. Res.*, 116,  
 707 D07102, <https://doi.org/10.1029/2010JD014891>, 2011.

708 Singh, M., Kumar, B., Chattopadhyay, R., Amarjyothi, K., Sutar, A.K., Roy, S., Rao, S.A., and Nanjundiah, R.S.:  
 709 Artificial intelligence and machine learning in earth system sciences with special reference to climate science and  
 710 meteorology in South Asia. *Current Sci.*, **122** (9), <https://doi.org/10.18520/cs/v122/i9/1019-1030>, 2022.

711 Steinacker, R., et al.: Unstationary aspects of Föhn in a large valley. Meteorology and Atmospheric Physics volume  
712 92, pages 255–284 (2006). <https://doi.org/10.1007/s00703-005-0134-y>, 2005.

713 Stohl, A.: Computation, accuracy and applications of trajectories - A review and bibliography, Atmos. Env., **32** (6),  
714 [https://doi.org/10.1016/S1352-2310\(97\)00457-3](https://doi.org/10.1016/S1352-2310(97)00457-3). 1998

715 Tenenbaum, J., Williams, P.D., Turp, D., Buchanan, P., Coulson, R., Gill, P.G., et al.: Aircraft observations and  
716 reanalysis depictions of trends in the North Atlantic winter jet stream wind speeds and turbulence. Quarterly Journal  
717 of the Royal Meteorological Society, 148(747), 2927–2941. <https://doi.org/10.1002/qj.4342>, 2022.

718 Tschannett, S.: Objektive hochaufgelöste Querschnittsanalyse. Diplomarbeit, Univ. Wien,  
719 <https://www.univie.ac.at/img-wien/>, 2003.

720 WMO: Guide to Instruments and Methods of Observation Volume I: Measurement of Meteorological Variables ,  
721 Commission for Instruments and Methods of Observation (CIMO) Guide, WMO Pub. 8. Available from  
722 <https://library.wmo.int/records/item/41650-guide-to-instruments-and-methods-of-observation>, 2021.

723 Zhang, J., Chen, H., Zhu, Y., Shi, H., Zheng, Y., Xia, X., Teng, Y., Wang, F., Han, X., Li, J., et al.: A Novel Method  
724 for Estimating the Vertical Velocity of Air with a Descending Radiosonde System. Remote Sens. **11**, 1538.  
725 <https://doi.org/10.3390/rs11131538>, 2019.